ADVANCED MATERIALS INTERFACES
www.advmatinterfaces.de

Fully Automated Optimization of Robot-Based MOF Thin Film Growth via Machine Learning Approaches

*Lena Pilz, Carsten Natzeck, Jonas Wohlgemuth, Nina Scheuermann, Peter G. Weidler, Ilona Wagner, Christof Wöll, and Manuel Tsotsalas**

Metal–organic frameworks (MOFs), have emerged as ideal class of materials for the identification of structure–property relationships and for the targeted design of multifunctional materials for diverse applications. While the powder form is most common, for the integration of MOFs into devices, typically thin films of surface anchored MOFs (SURMOFs), are required. Although the quality of SURMOFs emerging from layer-by-layer approaches is impressive, previous works revealed that the optimum growth conditions are very different between different types of MOFs and different substrates. Furthermore, the choice of appropriate synthesis conditions (e.g., solvents, modulators, concentrations, immersion times) is crucial for the growth process and needs to be adjusted for different substrates. Machine learning (ML) approaches show great promise for multi-parameter optimization problems such as the above discussed growth conditions for SURMOF on a particular substrate. Here, this work presents an ML-based approach allowing to quickly identify optimized growth conditions for HKUST-I SURMOFs with high crystallinity and uniform orientation. This process can subsequently be used to optimize growth on other types of substrates. In addition, an analysis of the results allows to gain further insights into the factors governing the growth of MOF thin films.

1. Introduction

Metal–organic frameworks (MOFs) are made by assembling metal nodes and organic linker molecules into highly crystalline, porous 3D networks.[1,2] The number of experimentally characterized MOFs, which are assembled from molecular building blocks, already exceeds 100 000, the maximum number is virtually unlimited.[3] Due to the large variability in composition and structure, MOFs are able to incorporate numerous functionalities, which makes these materials highly attractive for a wide range of applications. Important examples are gas storage and separation, catalytic reactions, fabrication of sensors, organic electronic devices, as well as life sciences applications, including drug delivery, and anti-bacterial surfaces.[4–10] Depending on the synthesis and processing conditions, the macroscopic form of MOFs can be rather different. While straight forward solvothermal synthesis commonly yields powder materials,[11,12] more sophisticated synthesis approaches yield large (up to one mm) single crystals or highly oriented MOF thin films.[13,14] In the case of MOF thin films, a variety of strategies are available that can even be used to produce monolithic thin films after careful optimization of the conditions.[15–19] The growth of oriented MOF thin films on functionalized interfaces is of pronounced interest, as the orientation of these crystalline highly anisotropic compounds strongly influence their performance in several applications.[20] Also, the integration of MOFs in electronic devices requires the fabrication of well-defined interfaces between MOFs and electrical conductors.[21,22] To meet these requirements, a wide variety of synthesis schemes have been developed, including vapor assisted conversion or chemical vapor deposition.[23,24] Some of the highest quality MOF thin films have been produced by the liquid phase layer-by-layer method, which yields monolithic thin film, referred to as surface anchored MOFs (SURMOFs) (see **Figure 1**).[25,26] SURMOFs can be grown with a high degree of crystallinity on a large variety of different substrates. In several cases it has been shown that SURMOFs have a lower density of defects than the corresponding bulk materials, for example, in the case of HKUST-1.[27] Different orientations strongly influence the final properties of the SURMOF, for example, in the context of anisotropic transport of excitons created by absorption of light.[28] The layer-by-layer process can also be used to realize MOF-on-MOF heteroepitaxial thin films, which are of interest, for example, in the context of photon up conversion.[29]

The large interest in controlling the crystallographic orientation of SURMOFs led to numerous studies on the influence of substrate functionalization and specific reaction parameters on the orientation as well as the crystal morphology. Liu et al. investigated the influence of differently functionalized

L. Pilz, C. Natzeck, J. Wohlgemuth, N. Scheuermann, P. G. Weidler, I. Wagner, C. Wöll, M. Tsotsalas
Karlsruhe Institute of Technology (KIT)
Institute of Functional Interfaces (IFG)
Hermann-von-Helmholtz-Platz 1
76344 Eggenstein-Leopoldshafen, Germany
E-mail: manuel.tsotsalas@kit.edu

The ORCID identification number(s) for the author(s) of this article can be found under https://doi.org/10.1002/admi.202201771.

DOI: 10.1002/admi.202201771

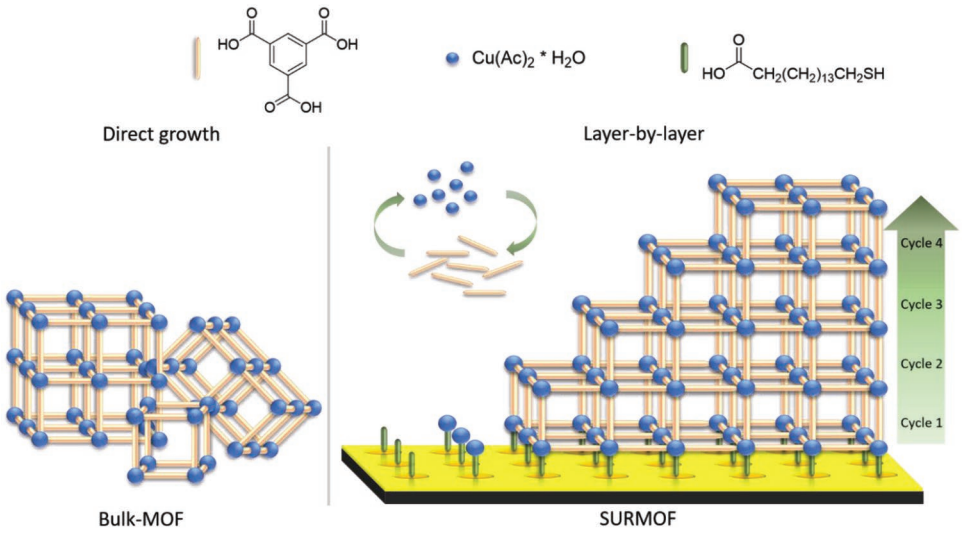

Figure 1. The reaction of metal nodes (blue spheres, dicopperacetate monohydrate for HKUST-I) with organic linker molecules (yellow bars, trimesic acid for HKUST-I) results in metal–organic frameworks (MOF). Depending on the synthesis method they are gained as diversely oriented bulk-MOFs powder (left side) or as highly oriented surface anchored MOFs (SURMOFs) by using the layer-by-layer growth method (right side). In the LbL method, a self-assembled monolayer (SAM, green bars) acts as a starting point for the SURMOF growth.

self-assembled monolayers (SAMs) on gold-coated substrate on the thin film orientation.[30] Zhuang et al. studied the influence of temperature on the crystal orientation.[31] Vello et al. examined the influence of the chain length of the SAM by keeping the functional group constant.[32] These previous studies have shown that there is a strong influence of surface functionalization on the orientation of these crystalline thin films. However, also for a given substrate a desired crystallographic orientation of SURMOFs can be obtained by the layer-by-layer liquid phase epitaxy after appropriate optimization of synthesis parameters. In some cases, also the sequence of the layer-by-layer-steps has a pronounced influence, even the orientation of the SURMOFs can be controlled.[33]

So far, optimization of MOF thin film properties has been mostly carried out by variation of a single parameter, as multi-parameter optimization is a highly complex approach. Since the SURMOF synthesis process is complex and the film properties depend sensitively on synthesis conditions, previous works have used time- and resource-intensive trial-and-error experiments, where usually only one synthesis parameter is optimized at a time. However, in view of the many parameters that influence MOF growth, the simultaneous variation of many parameters is required. We demonstrate here that such an optimization can be carried out using machine learning (ML) optimization tools. We have chosen a particular approach, the so-called "synthesis condition finder."[34] With this tool it is possible to optimize several synthesis parameters at the same time while pursuing several optimization objectives, that is, several properties of the product, at the same time. Thus, this is not only a multi-parameter but also a multi-objective optimization. In addition, the SyCoFinder tool allows to determine the relative importance of individual parameters for a particular MOF property.

To successfully apply machine learning optimization techniques in chemical synthesis, it is indispensable to use synthesis schemes which guarantee high reproducibility. To fulfill this requirement the synthesis of the SURMOFs studied here has been performed by a robotic system operated in a glovebox filled with inert gas. The robotic setup consists of several vessels arranged around the six-axis robot containing separate solutions of metal salt and linker along with the modulator and cleaning solutions (see Figure S1a, Supporting Information). Furthermore, there is an ultrasonic station and a spray cleaning station for additional cleaning of the samples. The robot performs a layer-by-layer synthesis by immersing the substrates functionalized with a SAM in the different solutions for a fixed time. The sequence of one cycle, in which a single layer is formed, starts with the metal-salt solution, followed by one or more cleaning steps, continues with the linker solution and after another cleaning step the next cycle is started (see Figure 1).[35,36]

The different synthesis parameters studied in this work were the metal and linker concentrations, the amount of the growth modulator (water), the cleaning time via ultrasonication, and the cleaning time via spray cleaning. In our approach all variables are part of the synthesis-process itself, but substrates as well as the SAM were strictly kept constant.

For the SURMOF synthesis, we are operating in a huge multi-parameter space (see **Figure 2**a), where the parameters of the synthesis constraints may depend on each other in unknown ways, it can be very tedious to find the optimum of the parameters using a classical optimization method where only one parameter can be optimized at a time. Machine learning approaches offer a solution to this problem, since the optimal combination in a multi-parameter space can be found rationally and efficiently.[37]

The integration of machine learning in material synthesis is not trivial. We showed that the use of synthesis conditions collected from literature can be employed for synthesis prediction, generating an "initial best guess."[38] However, for the following synthesis optimization step the experimental data needs to be of high quality. We therefore feel that for a reliable ML-based optimization, a robot station connected with genetic algorithms is a highly promising approach. A popular

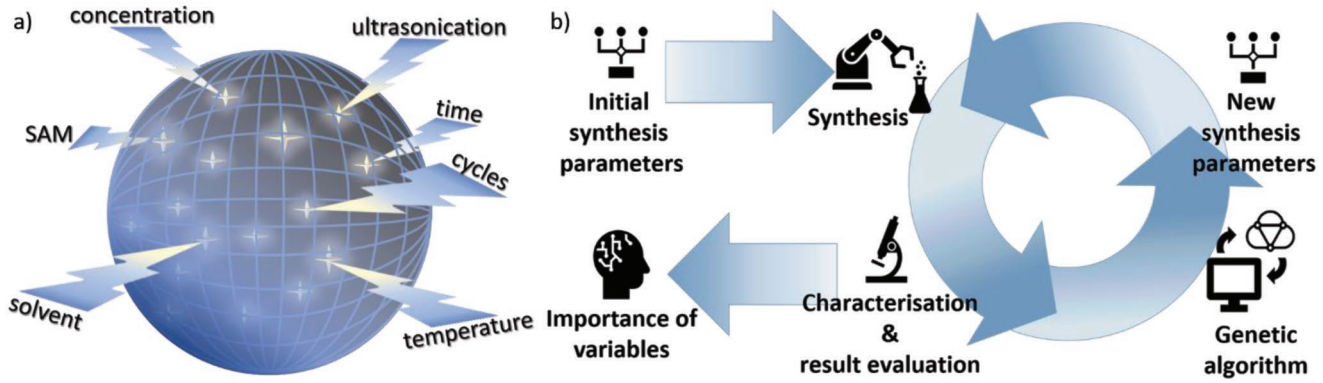

Figure 2. a) The sphere represents a multi parameter space where all the variables known as synthesis parameters, such as time, temperature, etc. have unknown and overlapping influences on the outcome of a synthesis. Depending on the desired properties of the synthesized compound the optimal combination of these variables is to be found somewhere in the multi parameter space via machine learning. b) The practical implementation of machine learning optimization starts with the initial synthesis parameter sets created in the diverse set. Those parameter sets are then synthesized and rated by characterizing and evaluating the results. The rated parameter sets are passed to the genetic algorithm, which recombines them and creates new, further optimized synthesis parameter sets. Those are again to be synthesized, characterized, and rated. This cycle is repeated until the results are satisfactory. Then all data is evaluated according to the importance of variables.

ML approach is SyCoFinder provided in the materials cloud platform, that uses genetic algorithms for synthesis optimization.[34] The SyCoFinder consists of three consecutive steps. In the first step, "Diverse Set," the space of parameters is defined, together with intervals in which they are allowed to vary. In order to obtain as diverse combinations of parameters as possible, the calculation of these parameter sets is performed by the so-called MinMax method. Here, one data point is randomly selected in the defined parameter space and all subsequent points are selected by calculating their furthest distance from each other. This ensures that the entire parameter space is covered with only a few samples. On this basis, the experimental syntheses are carried out and characterized. From these results, a so-called fitness value is computed, which can adopt values between 0 and 1. In the second step, a new set of synthesis parameters based on the diverse set is computed using the genetic algorithm. Evolution and optimization of generations is achieved by the genetic algorithm considering the parental chromosomes, which are the different sets of parameters, according to their calculated fitness values and recombining those that perform well. For more details and a deeper understanding of the genetic algorithm as well as the selection by the MinMax procedure, we refer the reader to Moosavi et al.[34] After successful synthesis and characterization of these further developed parameter sets, a new optimization cycle is started. The process ends when the characterization results are considered optimized (see Figure 2b), which is defined by criteria set by the user. In the last step, after termination of the optimization, all generated data are analyzed with regard to the importance of the parameters.[34]

For this study we used HKUST-1, a popular MOF that was first synthesized in 1999 by Chui et al. and is named after Hong Kong University of Science and Technology.[39] The metal center of the cubical HKUST-I system consists of a di-copper tetracarboxylate unit. The organic linker molecule to which the coordinating carboxylate groups around the copper atoms belong is trimesic acid (1,3,5-benzenetricarboxylic acid [BTC]).

2. Results and Discussion

2.1. Evolution of Preferred Orientation

Figure 3a shows the X-ray diffraction (XRD) pattern of a simulated HKUST-1 bulk-MOF (blue), with random orientation of the crystallites, as well as two characteristic diffractograms of oriented HKUST-I SURMOFs, with either the [100] (red) or the [111] (black) orientation perpendicular to the substrate. The X-ray diffractograms of the whole generations can be found in Graphs S4–S6). Figure 3b,c shows exemplary scanning electron microscope (SEM) images recorded for these two differently oriented MOF thin films. Figure 3b) nicely shows the octahedral shape corresponding to the [100] orientation of the HKUST-I-SURMOF, while Figure 3c shows the triangles typical for crystallites oriented along the [111] direction.

In **Figure 4** we show the evolution of parameters during a full optimization process. The average-fitness of the successful experiments increases over three synthesis generations (see Figure 4a). Since we want to control the growth of a certain orientation in a thin film it has been decided to consider the optimization as successful, when the desired orientation reaches 100%. Besides, a high crystallinity is required to ensure the quality of the sample and the target value was therefore set to minimum 80%, which means a total fitness of 80% in one sample is required. The Diverse Set (first generation) contains four successful experiments out of ten according to the predetermined criteria, that is, has a percentage of preferred orientation greater than zero compared to a simulated powder diffractogram and shows crystallinity and phase purity present. Within this generation there is already one very fortunate set of parameters (04-DS) resulting in a fitness of 0.77. However, the crystallinity of this sample amounts to only 78%, and further optimization is required. Although the second generation has a better fitness average than the first, it initially looks as if the results have deteriorated. Only two out of ten experiments achieve a fitness-value above zero and the best value from this

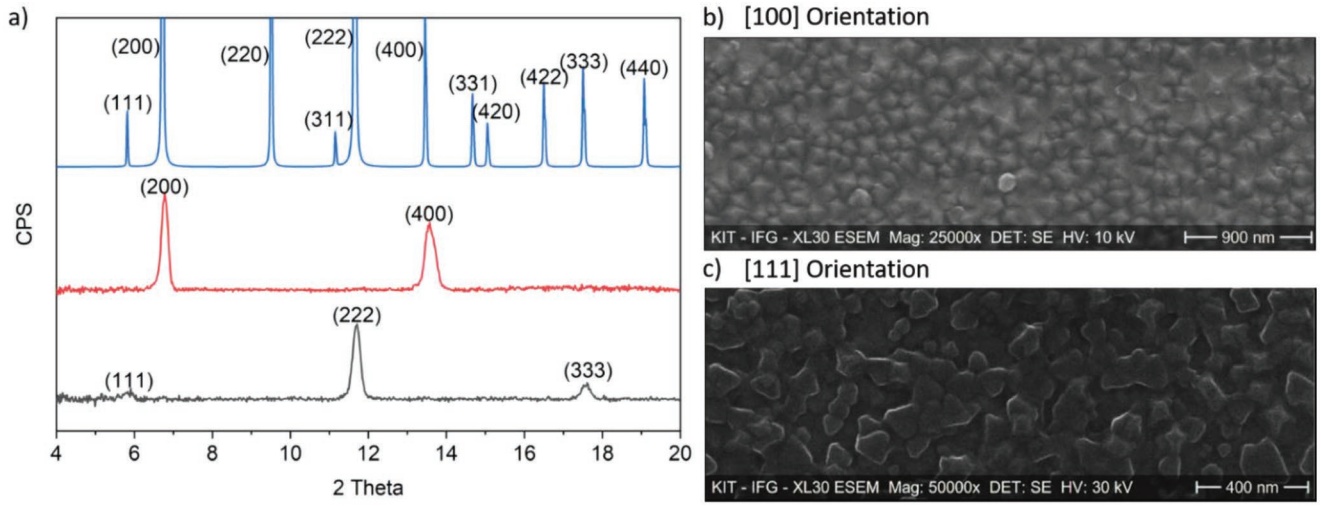

Figure 3. a) X-ray diffractograms of simulated bulk-MOF (blue) compared to oriented grown HKUST-I SURMOF in [100] direction (red) and [111] direction (black); b) SEM picture of oriented grown HKUST-I SURMOF in [100] direction; c) SEM picture of oriented grown HKUST-I SURMOF in [111] direction. The corresponding synthesis conditions can be found in the Supporting Information.

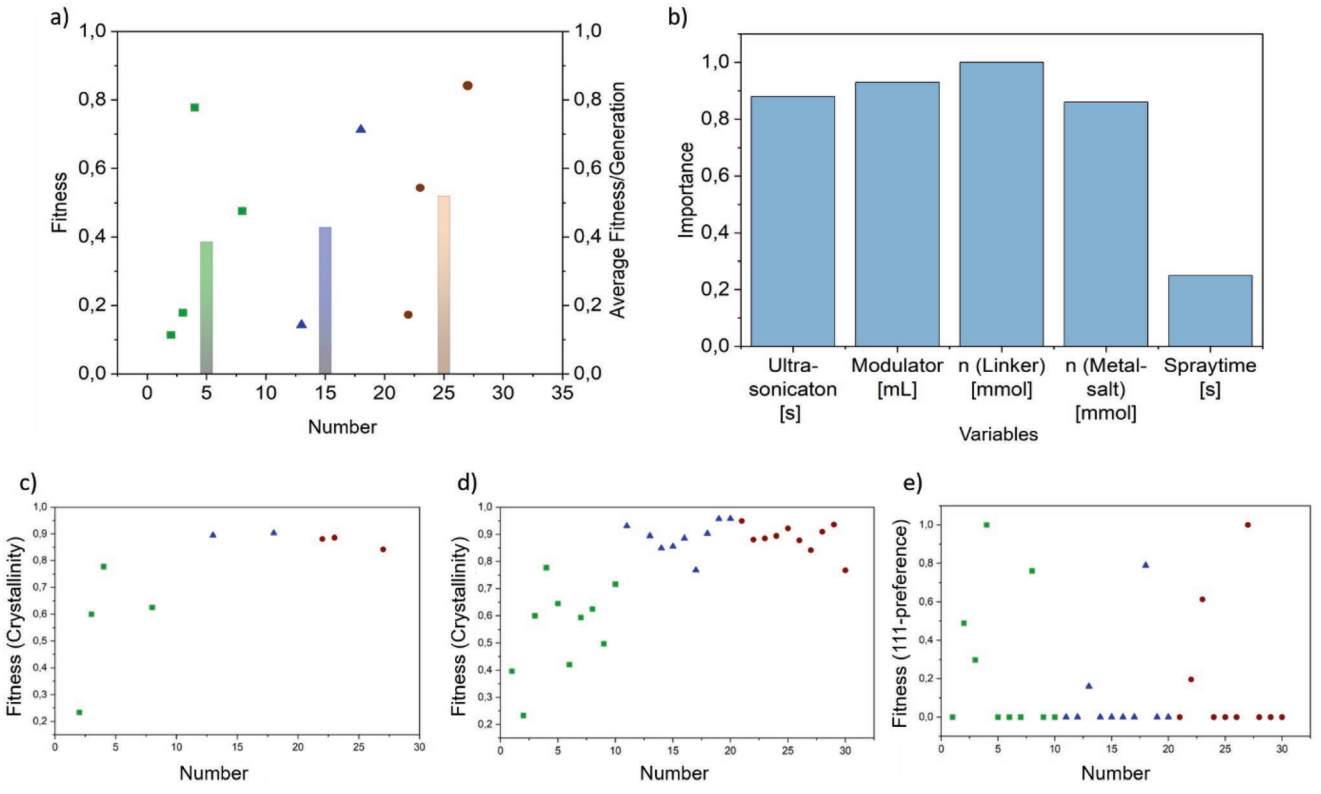

Figure 4. For a, c, d, and e the following legend is applied: the green squares belong to the first generation (Diverse Set), the blue triangles to the second (Genetic Algorithm 1) and the brown dots to the third generation (Genetic Algorithm 2), full size images of c, d, and e can be found in the Supporting Information (see Graphs S1–S3, Supporting Information). a) The data points represent the fitness-value of the successful experiments throughout the machine learning guided optimization; The bars show the average fitness of the successful experiments per generation in the same color code b) the importance of variables is shown for each variable used throughout the machine learning guided optimization; c) The development of the crystallinity of the successful experiments, that is, experiments also showing a preferred 111-orientation and therefore inheriting a fitness-value larger than zero, is shown over the three generations; d) The development of the crystallinity of all experiments yielding HKUST-1 but not necessarily with the desired 111-orientation over the three generations is shown here; e) The development of the preferred 111-orientation over the three generations is shown here.

Table 1. All successful parameter sets from the machine learning optimization ordered by decreasing fitness.

Fitness	Crystallinity [%]	[111]-Orientation [%]	Ultra-sonication [s]	Modulator [mL]	*n* (Linker) [mmol]	*n* (Metal-salt) [mmol]	Spray [s]
0.84	84	100	100	0.0	7.25	0.02	3
0.78	78	100	100	0.0	10.00	0.02	3
0.71	90	79	100	0.0	9.32	2.77	5
0.54	89	61	25	0.0	6.59	8.92	4
0.48	63	76	60	0.0	10.00	10.00	0
0.18	60	30	0	0.0	5.01	10.00	5
0.17	88	20	82	0.0	9.74	4.95	2
0.14	89	16	25	0.0	6.59	8.92	4
0.11	23	49	100	40.0	10.00	10.00	5

generation is below that of the diverse set. On closer inspection, however, in this generation the previously diversely distributed crystallinity has improved and is now around 90% for both samples (see Figure 4c). This improvement becomes even more evident when considering the crystallinity values of the entire generation if the criterion of the preferred orientation is temporarily disregarded (see Figure 4d). Since Figure 4d shows the crystallinity of all experiments where the phase purity criterion is satisfied, this also illustrates that 29 of 30 experiments yield HKUST-1 in principle. But it is evident from Figure 4e) that only nine of the 30 experiments also lead to the desired 111-orientation, which is therefore likely to be the more complex criterion to achieve and thereby realize a fitness value above zero. Due to this circumstance the increase of the average fitness of the generations from 0,38 in the first to 0,52 in the third generation is a significant step. The third generation also contains the best experiment with a fitness of 0.84. Split up into the single evaluation criteria it has a crystallinity of 84% and a perfect [111]-orientation of 100%. For visualization, SEM images were also taken from the best three samples (See Figure S2, Supporting Information).

2.2. Importance of Variables

After completion of the optimization process, the parameter sets of all generations together with their fitness values are returned to the synthesis condition finder to determine the importance of the selected variables. The importance of the variables is determined using an embedded random forest method, which is recommended for small data sets. It represents the influence of each variable on the target variable, while also considering possible influences of the variables on each other. In other words, it shows the strength of the relationship of the variables to the fitness values. The importance is estimated by observing the change in the prediction error when the values of one variable are permuted while the others are kept constant. For further details on the procedure of the random forest embedded method the reader is referred to Liaw and Wiener as well as Moosaavi et al.[34,40]

At first glance, the graph seems to reveal that all parameters except for the spray time are of great importance (see Figure 4b). Looking more closely now at the parameters of all nine successful syntheses (see **Table 1**), further insights can be gained on the HKUST-I SURMOF system and its orientation adjustment: Ordered by decreasing fitness, the first three sets of parameters show that the high importance of ultrasonic cleaning time means that it takes its maximum value. In agreement with the work of Gu et al.[36] we assume, that ultrasonication is responsible for the removal of unreacted components. This results in a smoother surface of the MOF, but as furthermore every layer is cleaned during the synthesis, it is therefore assumed that ultrasonication has a huge impact on the crystallinity. The nature of the importance of the amounts of metal and linker source, each taken separately, is not quite as obvious. But taken together and again considering the three best parameter sets, it becomes clear that for successful growth in the direction of [111], it is necessary to provide the linker source in a significant excess to the metal salt. In the case of the water parameter, it is the clearest: important here means having no water at all in the system, as eight out of nine syntheses agree on this parameter. This phenomenon can be explained according to Müller et al.[35] as well as Zhang et al.[41] when taking a look at the growth process of both orientations [100] and [111]. Both works agree that water as a modulator forms solvation shells and therefore is slowing down the bonding between copper atoms and carboxylic groups. When growing in [100] direction only two of those bonds form simultaneously, whereas three bonds are necessary for the formation of an [111]-orientation. Thus, if, as previously assumed, the formation of the aforementioned bond is inhibited by the presence of water, it stands to reason that the formation of only two bonds, that is, the [100] orientation is preferred as soon as water is present. It was also claimed in these studies that presence of water as modulator is necessary to obtain high crystallinity. However, here we can show that the simultaneous adjustment of multiple parameters also allows to obtain highly crystalline SURMOFs in [111] orientation.

2.3. Increasing Cycles

In the following we investigated whether the preferred orientation of the SURMOF growth continues for growth cycles exceeding the number of 40. The work of Njem et al.[42] showed very nicely, that for such larger numbers of deposition cycles the influence of underlying SAMs decrease and the formation of a preferred orientation such as [111] is lost. To challenge this assumption, we performed additional experiment with

80 instead of 40 deposition cycles, according to the optimized conditions. By adjustment of the orientation, without considering the SAM, by only varying synthesis-parameters, we found, that even at much higher cycle numbers the resulting X-ray diffractogram still shows a clear orientation of 92% in [111] direction with a crystallinity of 95% (see Graph S7, Supporting Information).

3. Conclusion

We have performed a multi-parameter and multi-objective optimization of HKUST-I SURMOF thin film synthesis on Au-substrates functionalized with an organo-thiolate SAM, focusing on both crystallinity and orientation of these MOF thin films. We performed the SURMOF synthesis following a layer-by-layer approach and optimized the parameters concentration of the metal source, concentration of the linker source, addition of water as modulator, sonication, and additional spray rinsing. The synthesis was performed using a fully automated robot system under inert conditions.

The results showed that by adjusting multiple parameters simultaneously, both [100] and [111] orientations of HKUST-I SURMOFs can be obtained in high crystallinity on carboxylic acid functionalized SAMs. The challenging simultaneous variation of multiple parameters was mastered very well by using a genetic algorithm, which requires only a few experiments for the huge parameter space resulting from five variables. In contrast to previous reports, our results clearly demonstrate that not only one parameter (e.g., water addition or substrate functionalization) is solely responsible for a certain orientation or for a high crystallinity, but multiple parameters are mutually important and several regions in the large multi-parameter space of the SURMOF synthesis can lead to high crystallinity with desired orientation. In addition, our results demonstrate that machine learning approaches, such as the employed genetic algorithm, are well suited to analyze this condition space both efficiently and effectively. By covering a large condition space under inert conditions using a reproducible, fully automated synthesis setup, we could challenge previous assumptions, based on studies focusing on only a very narrow parameter space, namely: 1) Addition of water is needed to obtain highly crystalline HKUST-I SURMOFs; 2) a certain surface modification is needed for HKUST-I orientation; 3) at larger cycle numbers, the growth in [100] orientation always dominates the growth in [111] orientation.

In future studies the optimization algorithm applied here can be used to, first, optimize HKUST-I growth also on other types of substrate, for example, functionalized polymer surfaces, modified glass or other dielectric substrate like ITO and even textile fibers. Second, this optimization process of course is not restricted to HKUST-I, it can also be applied to other MOF materials suited for the layer-by-layer process to yield SURMOFs, for example, UiO-66, ZIF 8 and pillared-layer systems.

In our study, we clearly demonstrate the potential of machine learning optimization approaches for the synthesis of complex out-of-equilibrium systems, such as the layer-by-layer SURMOF growth. The ability to cover a large multi-parameter condition space allows to gain deeper insights and understanding of the growth process, unavailable to studies focused on only a narrow region of the potential space, when only optimizing one parameter at a time. The complete dataset of the synthesis optimization, including all raw data and meta data, is published in the repository Chemotion. This study and the corresponding open datasets can serve as nucleation point for further automated and ML guided studies, involving different SURMOF structures and additional parameters, such as temperature, and additional objectives, such as low roughness, which will enable a deeper understanding of SURMOF and other layer-by-layer synthesis processes and their underlying principles.

4. Experimental Section

Synthetic Procedure: Every synthesis was carried out on a TX-60 6-axis dipping-robot from Stäubli in a nitrogen-filled glovebox. Gold-coated silicon-wafer pieces of 1×3 cm^2 served as substrates. Prior to mounting them on the sample holder (maximum capacity: 4 substrates) they were coated with an alkane-thiolate-based SAM by immersion into 16-mercaptohexadecanoic acid for 72 h.

For the various syntheses of HKUST-I, solutions of copper di-acetate monohydrate in 210 mL ethanol and 1,3,5-BTC in a mixture of water and ethanol (total volume 210 mL) were prepared. Homogeneous mixing was ensured by subjecting the solutions to ultrasonication. The respective amounts of substances are provided in the Supporting Information.

During the actual layer-by-layer synthesis the functionalized substrates were subsequently immersed into the different solutions in a fixed sequence. The general order of one layer-by-layer cycle is as follows: 1) Dipping in metal solution (10 min) – 2) cleaning step 1 (spray cleaning (0–5 s) and/or ultrasonication (s) and/or dip cleaning (5 min)) – 3) dipping in linker solution (15 min) – 4) cleaning step 2 – (spray cleaning (0–5 s) and/or ultrasonication (0–100 s) and/or dip-cleaning (5 min)).

Computational Procedure: For the computational part of the optimization the procedure provided by the SyCoFinder web application was followed, starting with the definition of the variables, their ranges and the amount of experiments. Based on this information the SyCoFinder provided the Diverse Set with ten sets of parameter combinations. After successful synthesis, characterization, and fitness calculation these parameter sets were given back to the web application together with their corresponding fitness values. On this basis the optimization via the genetic algorithm was performed by the recombination and mutation of the rated parameter sets and was again provided with a new generation of parameter combinations to synthesize, characterize, and rate. This evolution of the generations was performed twice until the results were considered satisfying.

Methods: The target properties, phase purity, crystallinity, and orientation were determined by XRD. In addition, control SEM (scanning electron microscopy) experiments were carried out to visualize the shape of the deposited crystallites.

Methods—X-Ray Diffraction: All diffractograms were recorded in the range from $2\theta = 3°$ to $2\theta = 20°$ using a Bruker D8 Advance diffractometer in θ–θ geometry, equipped with a LYNXEYE position sensitive detector with 192 active stripes. Additionally, the range from $2\theta = 37°$ to $2\theta = 40°$ was recorded in order to detect the characteristic substrate gold diffraction peak, which was used as a reference. All measurements were recorded with 2 s per step leading to 384 s total measuring time per step.

Every measurement was subjected to height error correction and background correction via DIFFRAC.EVA-software V. 5.2.0.3 provided by Bruker AXS. For the evaluation of crystallinity, a built-in routine by Bruker was applied. For the evaluation of phase purity, the diffractograms were compared to a simulated HKUST-I powder diffractogram.

Table 2. The parameters chosen as variables and their according ranges in which they are to be varied.

Parameter	Range
Metal salt quantity	0.02–10.00 mmol
Linker quantity	0.02–10.00 mmol
Amount of water (modulator)	0.0–40.0 mL
Cleaning time via ultrasonication	0–100 s
Cleaning time via spray-unit	0–5 s

Methods—Scanning Electron Microscopy: Prior to analysis by SEM, all samples were coated with 5 nm platinum with a Baltec MED-020 High Vacuum Coating System. All pictures were taken with a XL30 ESEM FEG (Environmental Scanning Electron Microscope XL30 Field Emission Gun), Fa. Philips in high vacuum mode between 10 and 30 kV.

Procedure: To achieve a highly crystalline and clearly oriented SURMOF five experimental parameters were varied: The concentrations of metal salt and organic linker, the cleaning times via ultrasonication and spray cleaning, and the amount of water as modulator. The ranges for each parameter are shown in **Table 2**. None of the parameters was weighted. The amount of experiments was set to ten for each generation.

Fitness: The crucial parameter for the genetic algorithm was the fitness value ranging between 0 and 1. In this work fitness was determined from crystallinity, phase purity, and orientation as determined by XRD and was computed according to

$$\text{fitness} = \text{fitness}(\text{phase purity}) \times \text{fitness}(\text{crystallinity}) \times \text{fitness}(\text{orientation}) \quad (1)$$

Here, phase purity is a simple binary criterion, which adopts a value of 1 if the phase corresponds a reference diffractogram of HKUST-I and 0 otherwise. As a result of this definition, any set of parameters not yielding the characteristic HKUST-I diffraction peaks was rejected. Three samples (m_1, m_2, m_3) were taken for each optimization step and used for averaging:

$$\text{fitness}(\text{phase purity}) = \frac{f_{m1} + f_{m2} + f_{m3}}{3} \quad (2)$$

"fitness (crystallinity)" was calculated from the global and reduced areas of the crystalline and amorphous signals corresponding to the integrals of the uncorrected and background subtracted data, respectively, in the diffractograms.

$$\text{Amorphous}[\%] = \frac{\text{Gobal area} - \text{Reduced area}}{\text{Global area}} \times 100 \quad (3)$$

$$\text{fitness}(\text{crystallinity}) = 100 - \%\ \text{Amorphous} \quad (4)$$

To quantify the intensity of domains with [111] orientation, the ratio ν_m of the signals m_{222} and m_{400} was compared with the intensity ratio ν_s of simulated diffractograms of randomly oriented samples. Since the published values of the simulated intensities of the selected signals differ, the average of these signals, s_{222} and s_{400}, is formed from three simulations.[43,44]

m_{222} = ∅ of intensity of 3 measurements of the signal (222)
m_{400} = ∅ of intensity of 3 measurements of the signal (400)
s_{222} = ∅ of intensity of 3 simulations of the signal (222)
s_{400} = ∅ of intensity of 3 simulations of the signal (400)

$$\nu_m = \frac{m_{222}}{m_{400}} \quad (5)$$

$$\nu_s = \frac{s_{222}}{s_{400}} = 5{,}19 \quad (6)$$

The creation of a fitness value for the orientation was made by a case distinction. This simply displays whether there was a positive deviation in the diffractogram of the SURMOF into [111] direction, meaning a preferred orientation, compared to the simulated randomly oriented diffractogram.

$$a)\ \text{for } \nu_m > \nu_s \text{ resp.} \left(\frac{\nu_s}{\nu_m}\right) \leq 1\text{: fitness (orientation)} = 1 - \left(\frac{\nu_s}{\nu_m}\right) \quad (7)$$

$$b)\ \text{for } \nu_m \leq \nu_s \text{ resp.} \left(\frac{\nu_s}{\nu_m}\right) > 1\text{: fitness (orientation)} = 0 \quad (8)$$

The original data is provided in the Chemotion repository.
Diverse Set: https://doi.org/10.14272/collection/LP_2022-07-28 [45]
Genetic Algorithm 1: https://doi.org/10.14272/collection/LP_2022-07-28_2[46]
Genetic Algorithm 2: https://doi.org/10.14272/collection/LP_2022-07-28_3[47]

Supporting Information

Supporting Information is available from the Wiley Online Library or from the author.

Acknowledgements

M.T. acknowledges funding from the Helmholtz Association's Initiative and Networking Fund (Grant VH-NG-1147). The authors further acknowledge support by the Helmholtz program "Materials Systems Engineering" (MSE) at the Karlsruhe Institute of Technology. C.W. acknowledges support from Deutsche Forschungsgemeinschaft (DFG, German Research Foundation) under Germany's Excellence Strategy—2082/1—390761711. The authors would also like to extend their sincere thanks to Nicole Jung (IOC, Karlsruhe Institute of Technology) and the Chemotion development team for their great cooperation and support.

Conflict of Interest

The authors declare no conflict of interest.

Data Availability Statement

The data that support the findings of this study are openly available in Chemotion-Repository at https://doi.org/10.14272/collection/LP_2022-07-28, https://doi.org/10.14272/collection/LP_2022-07-28_2, https://doi.org/10.14272/collection/LP_2022-07-28_3, reference number [45–47].

Keywords

automated syntheses, l-b-l, machine learning, metal–organic framework, optimizations, orientation control, thin films

Received: August 10, 2022
Revised: October 7, 2022
Published online:

[1] H. Furukawa, K. E. Cordova, M. O'Keeffe, O. M. Yaghi, *Science* **2013**, *341*, 1230444.
[2] H.-C. Zhou, J. R. Long, O. M. Yaghi, *Chem. Rev.* **2012**, *112*, 673.

[3] P. Z. Moghadam, A. Li, S. B. Wiggin, A. Tao, A. G. P. Maloney, P. A. Wood, S. C. Ward, D. Fairen-Jimenez, *Chem. Mater.* **2017**, *29*, 2618.
[4] B. Xiao, P. S. Wheatley, X. Zhao, A. J. Fletcher, S. Fox, A. G. Rossi, I. L. Megson, S. Bordiga, L. Regli, K. M. Thomas, R. E. Morris, *J. Am. Chem. Soc.* **2007**, *129*, 1203.
[5] N. L. Rosi, J. Eckert, M. Eddaoudi, D. T. Vodak, J. Kim, M. O'Keeffe, O. M. Yaghi, *Science* **2003**, *300*, 1127.
[6] J. Lee, O. K. Farha, J. Roberts, K. A. Scheidt, S. T. Nguyen, J. T. Hupp, *Chem. Soc. Rev.* **2009**, *38*, 1450.
[7] Z. Wang, A. Knebel, S. Grosjean, D. Wagner, S. Bräse, C. Wöll, J. Caro, L. Heinke, *Nat. Commun.* **2016**, *7*, 13872.
[8] A. H. Assen, O. Yassine, O. Shekhah, M. Eddaoudi, K. N. Salama, *ACS Sens.* **2017**, *2*, 1294.
[9] S. Wuttke, D. D. Medina, J. M. Rotter, S. Begum, T. Stassin, R. Ameloot, M. Oschatz, M. Tsotsalas, *Adv. Funct. Mater.* **2018**, *28*, 1801545.
[10] A. A. Talin, A. Centrone, A. C. Ford, M. E. Foster, V. Stavila, P. Haney, R. A. Kinney, V. Szalai, F. El Gabaly, H. P. Yoon, F. Léonard, M. D. Allendorf, *Science* **2014**, *343*, 66.
[11] Q. M. Wang, D. Shen, M. Bülow, M. L. Lau, S. Deng, F. R. Fitch, N. O. Lemcoff, J. Semanscin, *Microporous Mesoporous Mater.* **2002**, *55*, 217.
[12] M. Schlesinger, S. Schulze, M. Hietschold, M. Mehring, *Microporous Mesoporous Mater.* **2010**, *132*, 121.
[13] O. Shekhah, J. Liu, R. A. Fischer, C. Wöll, *Chem. Soc. Rev.* **2011**, *40*, 1081.
[14] N. Stock, S. Biswas, *Chem. Rev.* **2012**, *112*, 933.
[15] E. Biemmi, C. Scherb, T. Bein, *J. Am. Chem. Soc.* **2007**, *129*, 8054.
[16] D. Zacher, A. Baunemann, S. Hermes, R. A. Fischer, *J. Mater. Chem.* **2007**, *17*, 2785.
[17] Y. Yoo, Z. Lai, H.-K. Jeong, *Microporous Mesoporous Mater.* **2009**, *123*, 100.
[18] J. Reboul, S. Furukawa, N. Horike, M. Tsotsalas, K. Hirai, H. Uehara, M. Kondo, N. Louvain, O. Sakata, S. Kitagawa, *Nat. Mater.* **2012**, *11*, 717.
[19] P. Falcaro, K. Okada, T. Hara, K. Ikigaki, Y. Tokudome, A. W. Thornton, A. J. Hill, T. Williams, C. Doonan, M. Takahashi, *Nat. Mater.* **2017**, *16*, 342.
[20] M. Linares-Moreau, L. A. Brandner, T. Kamencek, S. Klokic, F. Carraro, K. Okada, M. Takahashi, E. Zojer, C. J. Doonan, P. Falcaro, *Adv. Mater. Interfaces* **2021**, *8*, 2101039.
[21] J. Liu, C. Wöll, *Chem. Soc. Rev.* **2017**, *46*, 5730.
[22] I. Stassen, N. Burtch, A. Talin, P. Falcaro, M. Allendorf, R. Ameloot, *Chem. Soc. Rev.* **2017**, *46*, 3185.
[23] E. Virmani, J. M. Rotter, A. Mähringer, T. von Zons, A. Godt, T. Bein, S. Wuttke, D. D. Medina, *J. Am. Chem. Soc.* **2018**, *140*, 4812.
[24] I. Stassen, M. Styles, G. Grenci, H. V. Gorp, W. Vanderlinden, S. D. Feyter, P. Falcaro, D. D. Vos, P. Vereecken, R. Ameloot, *Nat. Mater.* **2016**, *15*, 304.
[25] O. Shekhah, H. Wang, S. Kowarik, F. Schreiber, M. Paulus, M. Tolan, C. Sternemann, F. Evers, D. Zacher, R. A. Fischer, C. Wöll, *J. Am. Chem. Soc.* **2007**, *129*, 15118.
[26] Z. Wang, C. Wöll, *Adv. Mater. Technol.* **2019**, *4*, 1800413.
[27] K. Müller, K. Fink, L. Schöttner, M. Koenig, L. Heinke, C. Wöll, *ACS Appl. Mater. Interfaces* **2017**, *9*, 37463.
[28] R. Haldar, M. Jakoby, A. Mazel, Q. Zhang, A. Welle, T. Mohamed, P. Krolla, W. Wenzel, S. Diring, F. Odobel, B. S. Richards, I. A. Howard, C. Wöll, *Nat. Commun.* **2018**, *9*, 4332.
[29] R. Haldar, C. Wöll, *Nano Res.* **2021**, *14*, 355.
[30] J. Liu, O. Shekhah, X. Stammer, H. K. Arslan, B. Liu, B. Schüpbach, A. Terfort, C. Wöll, *Materials* **2012**, *5*, 1581.
[31] J.-L. Zhuang, M. Kind, C. M. Grytz, F. Farr, M. Diefenbach, S. Tussupbayev, M. C. Holthausen, A. Terfort, *J. Am. Chem. Soc.* **2015**, *137*, 8237.
[32] T. P. Vello, M. Strauss, C. A. R. Costa, C. C. Corrêa, C. C. Bof Bufon, *Phys. Chem. Chem. Phys.* **2020**, *22*, 5839.
[33] D. Zacher, K. Yusenko, A. Bétard, S. Henke, M. Molon, T. Ladnorg, O. Shekhah, B. Schüpbach, T. de los Arcos, M. Krasnopolski, M. Meilikhov, J. Winter, A. Terfort, C. Wöll, R. A. Fischer, *Chemistry* **2011**, *17*, 1448.
[34] S. M. Moosavi, A. Chidambaram, L. Talirz, M. Haranczyk, K. C. Stylianou, B. Smit, *Nat. Commun.* **2019**, *10*, 539.
[35] K. Müller, J. S. Malhi, J. Wohlgemuth, R. A. Fischer, C. Wöll, H. Gliemann, L. Heinke, *Dalton Trans.* **2018**, *47*, 16474.
[36] Z.-G. Gu, A. Pfriem, S. Hamsch, H. Breitwieser, J. Wohlgemuth, L. Heinke, H. Gliemann, C. Wöll, *Microporous Mesoporous Mater.* **2015**, *211*, 82.
[37] D. Carta, L. Villanova, S. Costacurta, A. Patelli, I. Poli, S. Vezzù, P. Scopece, F. Lisi, K. Smith-Miles, R. J. Hyndman, A. J. Hill, P. Falcaro, *Anal. Chem.* **2011**, *83*, 6373.
[38] Y. Luo, S. Bag, O. Zaremba, A. Cierpka, J. Andreo, S. Wuttke, P. Friederich, M. Tsotsalas, *Angew. Chem., Int. Ed.* **2022**, *61*, e202200242.
[39] S. S.-Y. Chui, S. M.-F. Lo, J. P. H. Charmant, A. G. Orpen, I. D. Williams, *Science* **1999**, *283*, 2050.
[40] A. Liaw, M. Wiener, **2002**, *2*, 5.
[41] B. Zhang, J. Zhang, C. Liu, X. Sang, L. Peng, X. Ma, T. Wu, B. Han, G. Yang, *RSC Adv.* **2015**, *5*, 37691.
[42] N. Nijem, K. Fürsich, S. T. Kelly, C. Swain, S. R. Leone, M. K. Gilles, *Cryst. Growth Des.* **2015**, *15*, 2948.
[43] A. A. Yakovenko, J. H. Reibenspies, N. Bhuvanesh, H.-C. Zhou, *J. Appl. Crystallogr.* **2013**, *46*, 346.
[44] O. Kozachuk, K. Yusenko, H. Noei, Y. Wang, S. Walleck, T. Glaser, R. A. Fischer, *Chem. Commun.* **2011**, *47*, 8509.
[45] L. Pilz, *Chemotion-Repos* **2022**, 10.14272/COLLECTION/LP_2022-07-28.
[46] L. Pilz, *Chemotion-Repos* **2022**, 10.14272/COLLECTION/LP_2022-07-28_2.
[47] L. Pilz, *Chemotion-Repos* **2022**, 10.14272/COLLECTION/LP_2022-07-28_3.